

Hard-sphere random-packing model for an ionic glass: Yttrium iron garnet

M. E. Lines

Bell Laboratories, Murray Hill, New Jersey 07974

(Received 17 May 1979)

A computer model for amorphous yttrium iron garnet has been constructed using a modification of a method pioneered by Bennett involving the sequential addition of hard spheres. The method is embellished to allow for the presence of local electrostatic forces which are assumed to keep neighboring ions of like charge as far apart as the basic building algorithm will allow. This distance (between ion centers), for amorphous YIG, is $d = 2.4 \text{ \AA}$. The electric-field-gradient distribution at the iron sites is calculated in a point-charge approximation and provides an excellent interpretation of the observed Mössbauer quadrupole line shape in the paramagnetic phase. Ion-pair correlation densities out to a range of 10 \AA have been computed for all combinations of the constituent species. Finally the distribution of iron-oxygen-iron bond angles is computed and from this, via superexchange theory, a qualitative knowledge of the exchange distribution is obtained. This suggests that the magnetic properties of vitreous YIG may resemble those of a dilute antiferromagnet near its critical concentration.

I. INTRODUCTION

Amorphous solids can usefully be categorized in terms of the dominant chemical bond present. Thus metallic, ionic, and covalent bond types each have characteristic requirements which mold the near-neighbor configurations in the amorphous state. Coordination numbers are largest in amorphous metals where close packing is a characteristic feature. Structures of covalent amorphous semiconductors, on the other hand, have much smaller coordination numbers dictated by the need of each atom to satisfy a small number of strongly directional bonds. There is an extensive literature on both metallic and covalent amorphous materials with theoretical models (of the random-dense-packing and the continuous-random-network types, respectively) well developed for each.¹ In comparison, amorphous ionic materials have received far less attention and, although it seems physically apparent that the requirements of local charge neutrality will ensure the cations (anions) will in general be surrounded by anion (cation) polyhedra, no computer model prepared specifically for an ionic glass has (to our knowledge) yet been presented and tested with respect to any of its quantitative predictions.

The lagging of interest in ionic glasses has resulted primarily from the fact that most simple ionic materials are not good glass formers in the absence of extraneous network-forming additives. Nevertheless, several well-characterized amorphous oxides have recently been prepared by roller quenching from the melt without the addition of any extraneous glass formers.²⁻⁴ With the preparation of such samples it now seems an appropriate time to attempt to advance

the theoretical understanding of ionic glasses, particularly with respect to the role played by electrostatic forces in molding the local configurations.

The present work was triggered by the preparation by Gyorgy *et al.*⁴ of roller-quenched vitreous yttrium iron garnet, $\text{Y}_3\text{Fe}_5\text{O}_{12}$ (YIG). Essentially pure vitreous platelets were obtained which, upon crystallization, had the properties of stoichiometric YIG. Although one would perhaps have preferred a binary rather than a ternary material on which to pioneer a model for an ionic glass, YIG does have the advantages of being magnetic (and hence open to magnetic probing of both local and bulk properties) and of being very thoroughly investigated in its crystalline form. The passage to the vitreous state has very pronounced effects on the magnetism. Crystalline YIG is a high-temperature ferrimagnet with Curie temperature $T_C \approx 550 \text{ K}$ while its amorphous equivalent does not acquire a bulk magnetic moment at any temperature.⁴ Some spin-ordering transition (probably to an antiferromagnetically aligned phase) does take place at about 30 K although a detailed study of the ordered phase has not yet been reported. Mössbauer measurements⁴ confirm some type of spin ordering below 30 K , establish the valency $+3$ for the iron ions, and most importantly, from the point of view of the present paper, provide an accurate measure (via the paramagnetic quadrupole spectra) of the electric-field-gradient (EFG) distribution at the ferric nuclear sites.

In this paper we construct a computer model for amorphous YIG using a modification of the basic method pioneered by Bennett using sequential addition of hard spheres.^{1,5} The present techniques for modeling amorphous structures are basically of two

types corresponding to the extremes of strongly covalent directional bonding (network models) and of spherically symmetric atoms (spherical packing models). Though many materials do not fit neatly into either of these categories it seems clear that ionic materials with formally filled outer electron shells can best be approached from the latter standpoint.

Dense-random-packing models which incorporate hard spheres of two or more sizes have already appeared in the literature in the context of amorphous alloys.⁶ In an ionic context it is necessary to embellish these in a manner which recognizes that local electrostatic repulsion will tend to keep neighboring ions of like charge as far apart as the sequential building scheme will allow. For YIG, in which the anions are large [oxygen radius $R(O) \approx 1.4 \text{ \AA}$] and the cations smaller [$R(Y) \approx 1.0 \text{ \AA}$ and $R(Fe) \approx 0.5-0.6 \text{ \AA}$] we find that it is not possible to build in the Bennett spirit without allowing for some anion-anion contact but that one can readily exclude contact between cations. Going further one can build sequentially maintaining a separation d between cation centers up to a maximum value $d = 2.4 \text{ \AA}$ beyond which the building scheme will not propagate. This maximum local separation of the trivalent cations then represents in some manner a minimization of local electrostatic energy within the building algorithm.

Our main contact with experiment in this paper is via a calculation of the electric-field-gradient distribution at the iron sites in the resulting amorphous aggregate. This field gradient (EFG) is a very sensitive function of the distance d (or of local electrostatic energy) both in distribution shape and in mean value. A quantitative agreement with the Mössbauer quadrupolar data in the $d = 2.4 \text{ \AA}$ limit lends some credence to the overall model and particularly to the necessity of recognizing the role played by electrostatic forces in molding the local configurations.

We also report computations of radial distribution functions out to 10 \AA for all combinations of ion-pair correlations (i.e., Y-Y, Y-Fe, Y-O, Fe-Fe, Fe-O, and O-O), predictions which could possibly be tested using extended x-ray absorption fine structure (EXAFS) techniques. Finally we examine the local Fe-O-Fe geometry within the model, establish the probability distribution of nearest-neighbor magnetic ions (defined as sharing a common oxygen ligand), and qualitatively estimate the expected exchange energy distribution in the hope that this might eventually lead to some understanding of the magnetic properties. In particular a close correspondence with dilute antiferromagnetism is suggested.

II. COMPUTER MODEL

Although the degree of ionicity of the bonds in YIG may be in question, the fact that Y is essentially

close packed in crystalline YIG while the iron sits fairly equally (in fact in a ratio of 3:2) in both tetrahedral and octahedral sites in the crystal^{7,8} establishes that hybridization or strongly directional bonding does not play a dominant role. In the crystal the mean Y-O bond length is 2.40 \AA (varying between 2.37 and 2.43 with Y in a distorted dodecahedral site) while the Fe-O bond lengths are 2.00 \AA at the octahedral sites and 1.88 \AA at the tetrahedral sites.⁷ Using the conventional radius $R(O) = 1.40 \text{ \AA}$ for oxygen, this establishes an yttrium radius $R(Y) = 1.00 \text{ \AA}$ relevant for YIG. For the ferric ion we find two values, corresponding, respectively, to the more covalent tetrahedral site and the less covalent octahedral site, of 0.48 and 0.60 \AA . Since we do not wish to differentiate between ferric ions in the glass (the Mössbauer data⁴ show a well-defined single-peaked EFG at the iron sites) we take the mean value $R(Fe) = 0.54 \text{ \AA}$ to be representative of ferric ions in amorphous YIG in a hard-sphere approximation.

Spherical systems have been extensively explored in the literature⁹ and many algorithms used to construct new models in the computer. Perhaps most widely used is the sequential addition method in which a sphere is brought up into contact with (initially) a pre-existing seed, and allowed to take up a position touching three others. In the "global" criterion, which we shall use, the particular "pocket" occupied by each added sphere is that closest to a preselected origin or center of the seed. The resulting boundary is then free and essentially spherical.

In detail our procedure is as follows. The seed cluster is made up of two oxygen spheres and one iron sphere all in contact in the $x-y$ plane with the center of one oxygen sphere taken as the origin [or more accurately as the point $(0,0,10^{-5} \text{ \AA})$], a procedure which removes the z , $-z$ symmetry, and prevents the occurrence of pockets which are accidentally equidistant from the origin]. We use throughout the criterion that no two cations may touch or even come closer together than an initially arbitrary center to center distance d . Starting from the above seed we first compute the possible positions for a new oxygen sphere in contact with the three spheres of the seed. The first pockets must be oxygen pockets since they involve contact with a cation, the seed ferric ion. Thus the "seed pocket" calculation results in a "substrate" of $N = 3$ ions and the positions of $M = 2$ new sites or pockets for an additional ion. Labeling all substrate ions and pockets according to their type (Y, Fe, or O) and formal valence charge ($3+$, $3+$, $2-$, respectively) the following procedure is now general for general N and M .

We first choose the global pocket and fill it so long as it does not result in a violation of the cation-cation distance criterion. If it does we strike out this pocket and proceed to the next global pocket until one is

found which does not violate this criterion. After filling this pocket we strike out all pockets which overlap the added $(N + 1)$ th sphere and proceed to a computation of the newly created pockets involving this $(N + 1)$ th sphere. In this respect we must first locate the eligible base triads involving the $(N + 1)$ th sphere and decide what type of new pocket is required. The triads are of two types—either they involve cations or they do not. In the former case we must add oxygen pockets since to add cation pockets would be to violate the cation touching and distance criteria. For triads containing three oxygen ions we decide the new pocket type as follows. First we calculate the charge on the existing substrate; if it is positive we compute oxygen pockets, if it is negative we calculate the existing Y to Fe ratio in the substrate and choose that cation (for the pocket computation) which will bring this ratio closer to its formal crystalline value 3:5. After calculating all the new pockets we strike out those which overlap the existing substrate. We now redefine N and M to represent the new substrate and pocket sets and repeat the entire procedure.

The method of choosing the pocket types ensures that the resulting amorphous aggregate grows with charge balance and with a correct proportionality of Y to Fe. Using about one hour of computer time on the Honeywell 6000 computer we were able to grow aggregates of about 750 spheres for several different values of d . As d is increased the fraction of cation pockets excluded by the distance criterion increases until, beyond some critical maximum $d = d_c$, all the available pockets are excluded at some stages of the growing process and the building process terminates. We found that a cluster of 748 ions could be grown

with $d = 2.4 \text{ \AA}$ (with cluster size limited by computer time restriction only) but for $d = 2.5 \text{ \AA}$ the building ceases at $N = 20$ at which point no pockets remain which satisfy the d criterion. The value of d_c therefore lies between 2.4 and 2.5 \AA for our sphere sizes.

III. DENSITY AND PACKING FRACTION

The room-temperature lattice constant of crystalline YIG is 12.376 \AA and there are eight formula units in the cubic unit cell.⁷ The volume per atom in the crystal is therefore 11.847 \AA^3 . The amorphous computer sample grows with a surface boundary which is approximately spherical in shape although some iron pockets, since $R(\text{Fe})$ is so small, are occasionally created and filled at "depths" of up to 1.7 \AA inside the "surface" defined by the larger ions. In Table I we quote the final composition and dimensions for three representative clusters built according to the directions of Sec. II. The first (*A*) was assembled without any d restriction although cation contact was prohibited; the second (*B*) and third (*C*) are with $d = 1.5$ and 2.4 \AA , respectively. The Y to Fe to O composition ratios are seen to be very close to the formal values 3:5:12 in all cases.

Defining the cluster radius $r(N)$ as a function of N by the most smoothly varying largest ion (oxygen) values alone, a typical convergence (actually for $d = 2.4 \text{ \AA}$) for reciprocal density $4\pi r^3(N)/3N$ as a function of $1/N$ is shown in Fig. 1. As can be seen, limiting values $1/N \rightarrow 0$ can be obtained with an accuracy of about $\pm 2\%$. From Table I we see that the glass density for no d criterion is essentially equal to the crystalline density. As we increase d and allow for near-neighbor cation electrostatic repulsion the

TABLE I. Basic data for three computer-assembled clusters *A*, *B*, and *C*. Cluster *A* is constructed with a simple restriction of no cation-cation contact. Clusters *B* and *C* add to this an additional requirement that no cation centers can approach closer than a distance d . Hard-sphere radii $R(\text{Fe}) = 0.54 \text{ \AA}$, $R(\text{Y}) = 1.00 \text{ \AA}$, $R(\text{O}) = 1.40 \text{ \AA}$.

d	Cluster <i>A</i>	Cluster <i>B</i> 1.5 \AA	Cluster <i>C</i> 2.4 \AA
Total number of ions, N_0	479	748	748
Number of Y ions, $N_0(\text{Y})$	73	115	112
Number of Fe ions, $N_0(\text{Fe})$	121	185	187
Number of O ions, $N_0(\text{O})$	285	448	449
$N_0(\text{Y})/N_0$ (ideally 0.150)	0.152	0.154	0.150
$N_0(\text{Fe})/N_0$ (ideally 0.250)	0.253	0.247	0.250
Cluster diameter $2r(N_0)$	$\approx 21.9 \text{ \AA}$	$\approx 25.7 \text{ \AA}$	$\approx 26.1 \text{ \AA}$
(density) ⁻¹ = $L^3 \frac{4\pi r^3(N)}{3N}$	$11.92 \pm 0.25 \text{ \AA}^3$	$12.05 \pm 0.25 \text{ \AA}^3$	$12.45 \pm 0.25 \text{ \AA}^3$
Packing fraction f	0.645	0.638	0.618

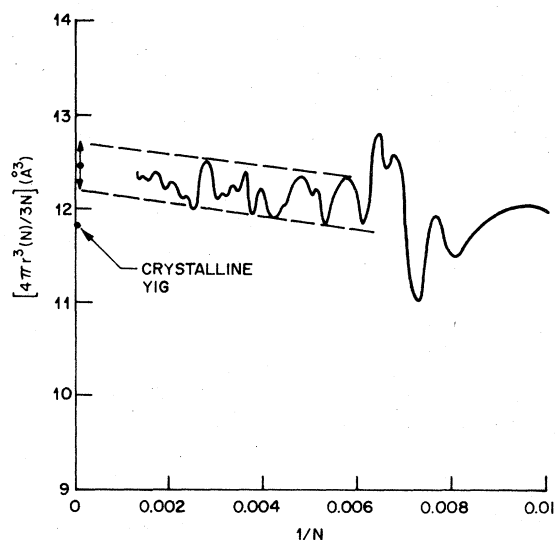


FIG. 1. Reciprocal density $4\pi r^3(N)/3N$ as a function of $1/N$ for cluster model C (with $d = 2.4 \text{ \AA}$) where $r(N)$ is the magnitude of the radius vector for the position of the N th ion. The curve connects only the points for the largest (oxygen) sphere positions since these are the least erratic and provide the best estimate for convergence to $1/N \rightarrow 0$. Also shown on the ordinate axis is the reciprocal density for crystalline YIG.

glass density decreases until, at the value $d = 2.4 \text{ \AA}$ which we believe to be most physically realistic, its value is some $5 \pm 2\%$ less than the crystalline equivalent. Experimentally we do not yet have an accurate measure of density for the vitreous YIG samples. From the extrapolated ($1/N \rightarrow 0$) density values, the sphere radii, and their proportional concentration we readily calculate a packing fraction f (defined as the fraction of the space occupied by spheres) which is also shown in Table I.

IV. EFG AT THE IRON SITES

In this section we use a point-charge model, with formal valence charges $z(\text{Y}) = z(\text{Fe}) = +3e$ and $z(\text{O}) = -2e$, to compute the matrix $V_m'' = \partial^2 V_m / \partial x_i \partial x_j$ ($i, j = 1, 2, 3$) of the second derivatives of the electrostatic potential V_m at the iron sites m with respect to the coordinate axes x_i . Diagonalizing V'' at each magnetic site to obtain its diagonal elements V_{11}, V_{22}, V_{33} , we define V_{11} as the largest value of $|V_{ii}|$ and a positive definite asymmetry parameter $\eta = (V_{22} - V_{33})/V_{11}$ for each such site in the various cluster samples. The convergence of the quadrupole sum is quite rapid and an accuracy of about ± 0.1 (in units of $e/\text{\AA}^3$) can be obtained in most cases summing out to only 3 \AA . Convergence can be tested for the innermost ferric ions out to radii of order 10 \AA . Sampling over all iron sites more distant than 3 \AA from the cluster surface (typically 80 to 90 sites for

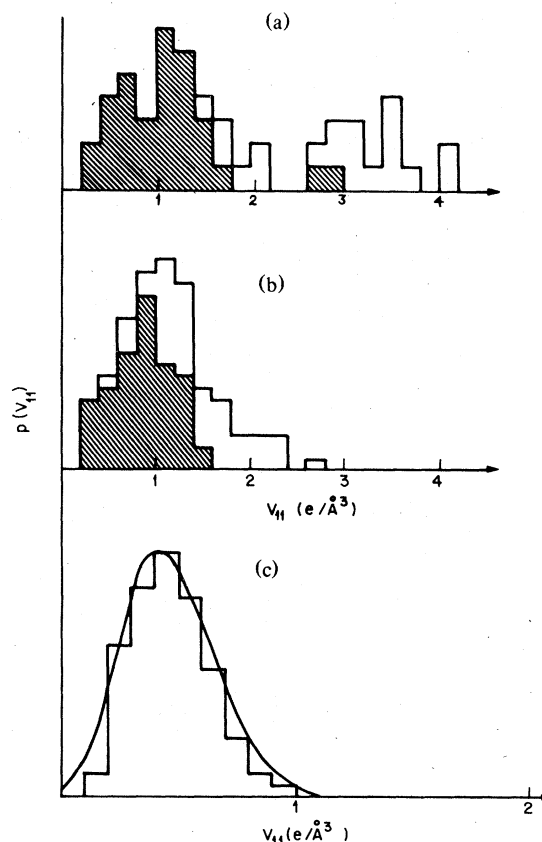


FIG. 2. Histograms for the probability distribution $p(V_{11})$ of iron-site EFG matrix element V_{11} for the three computer models A , B , and C [see (a)–(c), respectively] defined in Table I. Shown shaded for model A is the distribution if iron sites with nearest-neighbor cations (primarily iron) closer than 1.6 \AA are excluded. Shown shaded for model B is the distribution if sites with nearest-neighbor cations closer than 1.8 \AA are excluded. For model C (note the change of scale on the abscissa for this histogram) we also show the EFG distribution calculated from the observed Mössbauer quadrupole line shape (see text).

the larger clusters) we obtain the distributions shown in Fig. 2 for the A , B , and C clusters of Table I.

The EFG distribution is seen from Fig. 2 to be an extremely sensitive function of the closest cation approach allowed by the building algorithm. In cluster A , for which Fe ions can approach arbitrarily closely without touching (effectively $d = 1.08 \text{ \AA}$) the distribution is two peaked. One easily verifies from the computer calculation that the larger V_{11} contributions result from iron ions which have very close iron neighbors. In fact [see shaded in Fig. 2(a)] the higher V_{11} peak essentially disappears if we remove all contributions from iron sites with cation (primarily iron) neighbors closer than 1.6 \AA . Since the experimental Mössbauer quadrupole spectra⁴ establish quite

clearly the existence of a single-peaked V_{11} distribution in the roller-quenched YIG samples, it follows that no such near-neighbor iron-cation pairs exist in the real materials. Evidently the electrostatic repulsion between cations prevents the formation of cation pairs closer than a certain distance d .

In computer cluster *B*, with $d = 1.5 \text{ \AA}$ [Fig. 2(b)], only a single V_{11} distribution occurs in qualitative accord with experiment. Nevertheless, even here the width and extent of the distribution is still acutely sensitive to the near-neighbor iron-cation distribution. If, for example [shaded in Fig. 2(b)] we exclude contributions from iron sites with cation (Y or Fe) neighbors closer than 1.8 \AA , the mean value of EFG is reduced by more than 20%. Physically it seems likely that the best value to take for d is the largest for which the cluster building process will still take place, since this minimizes in some sense the local electrostatic energy within the confines of the model. As discussed earlier this limiting value is $d = 2.4 \text{ \AA}$. The EFG distribution for this case (cluster *C*) is shown in Fig. 2(c). The mean and peak values of V_{11} have been reduced by more than a factor 2 from Fig. 2(b).

Since the splitting of the Mössbauer quadrupole peaks provides a good measure of the peak $(V_{11})_{\max}$ in the V_{11} distribution we may now verify by direct calculation that the representation in Fig. 2(c) is indeed close to the correct one. The peak-to-peak quadrupole separation is 1.05 mm/sec or 12.2 MHz . It can be expressed¹⁰

$$\left(\frac{1}{2}\right)eQ(V_{11})_{\max}\left(1 + \frac{1}{3}\eta^2\right)^{1/2}(1 - \gamma_{\infty}) = 12.2 \text{ MHz} \quad (1)$$

in which $(1 - \gamma_{\infty})$ is the Sternheimer antishielding factor for Fe^{3+} and Q is the quadrupole moment of ^{57}Fe . The most accurate values presently available for $1 - \gamma_{\infty}$ and Q are 11 ± 1 and $0.15 \times 10^{-24} \text{ cm}^2$, respectively.^{11,12} Although the mean value of the asymmetry parameter is quite high (see below) the factor $(1 + \frac{1}{3}\eta^2)^{1/2}$ varies only between 1 and 1.15 at its extremes ($\eta = 0, 1$) and we can use the value 1.1 for it without concerning ourselves with the actual η distribution at this point. With these values, and an electronic charge $e = 4.8 \times 10^{-10} \text{ esu}$, we calculate

$$(V_{11})_{\max} = 0.39e/\text{\AA}^3 \quad (2)$$

directly from Eq. (1) in excellent agreement with Fig. 2(c). We conclude that the computer cluster *C* is the most physically relevant of our models and is to be used for any further predictions or comparison with experiment.

In Fig. 3 we show the probability distribution histogram $p(\eta)$ for field gradient asymmetry parameter η

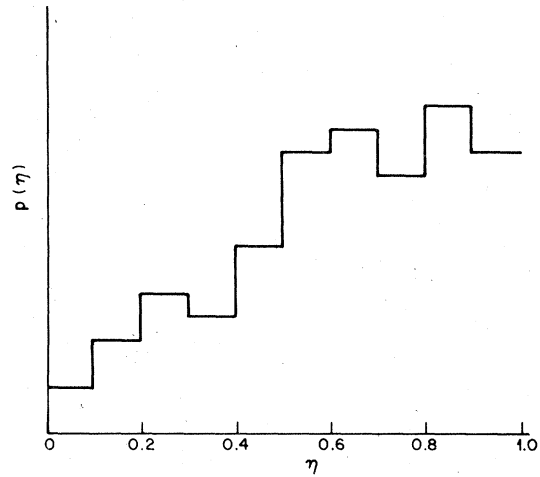


FIG. 3. Histogram of the probability distribution $p(\eta)$ of EFG asymmetry parameter η for computer model *C*.

using model *C*. The distribution appears to be a monotonically increasing function of asymmetry and may well approach zero as $\eta \rightarrow 0$. Thus, combining $p(V_{11})$ and $p(\eta)$ there is a definite tendency for glass to avoid high-symmetry EFG sites of any kind.

The linewidth of the individual Mössbauer lines that make up the quadrupole-split (QS) doublet in the disordered magnetic regime is large compared with the natural Lorentz linewidths expected for a sharp line. In terms of the full width at half maximum the observed linewidth is 0.71 mm/sec (8.24 MHz) compared with the natural Lorentz width $w \approx 0.20 \text{ mm/sec}$. It follows that the quadrupole line shape must, for this case, already be an approximate (slightly broadened) measure of actual EFG distribution in the glass. Theoretically we merely have to perform a Lorentz broadening calculation to establish a fairly quantitative determination of actual EFG distribution in the glass.

From Fig. 2(c) we expect a reasonable representation for the EFG distribution to be obtainable in terms of an asymmetric Gaussian. We try

$$p(V_{11}) = A_1 \exp\left[-\left(\frac{V_{11} - V_M}{aV_M}\right)^2\right], \quad V_{11} < V_M \quad (3)$$

$$p(V_{11}) = A_1 \exp\left[-\left(\frac{V_{11} - V_M}{bV_M}\right)^2\right], \quad V_{11} > V_M,$$

where V_M is the value of V_{11} for which $p(V_{11})$ is maximum, A_1 is an amplitude factor, and a and b are dimensionless constants. In terms of this distribution we calculate a Lorentz broadened symmetric quadrupole doublet line shape in the form

$$f(y) = A_2 \int_{-\infty}^{\infty} \frac{(w/2)^2 \exp\{-[(|V_{11}| - V_M)/xV_M]^2\} dV_{11}}{(w/2)^2 + (y - V_{11})^2} \quad (4)$$

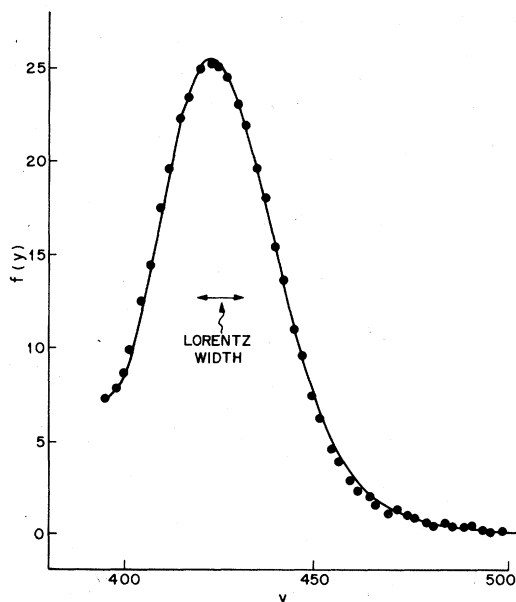


FIG. 4. Best theoretical fit (full curve) using Eq. (4) to the experimental Mössbauer line shape (filled circles). The amplitude parameter is arbitrary while the abscissa is measured in channel units of 0.01881 mm/sec per channel. Experimental data from Ref 4 and M. Eibschutz (private communication).

in which A_2 is an amplitude factor, y runs between $-\infty$ and ∞ , Lorentz width $w = 0.20$ mm/sec, and $x = b$ when $|V_{11}| > V_M$, and $x = a$ when $|V_{11}| < V_M$. Using Eq. (4) the best fit of theory with experiment is shown in Fig. 4 and gives values $V_M = 0.49$ mm/sec (5.7 MHz), $a = 0.54$, and $b = 0.85$. The distribution $p(V_{11})$ represented by these values of a and b is shown in Fig. 2(c) and accords very convincingly with the computer histogram for this same function. As seen from Fig. 4 the fit to the QS line shape is quite good. The corresponding best fit becomes worse if w is significantly increased from its natural linewidth value lending additional credibility to the entire fitting procedure.

V. PAIR-CORRELATION FUNCTIONS

In this section, using computer model $C(d = 2.4 \text{ \AA})$ we compute the various ion-ion correlation functions out to a range of 10 \AA . Consider a particular atom of type α (i.e., $\alpha = \text{Y, Fe, O}$). We compute the average density $g_{\alpha\beta}(r)$ of ions of type β at a distance r from ions of type α . In a continuum model this correlation function is both independent of α and r and is easily calculated in terms of the total material density ρ in the form

$$g_{\alpha\beta}(\text{continuum}) = c_{\beta\rho} \quad (5)$$

where $c_{\beta} = N_0(\beta)/N_0$ is the relative concentration of

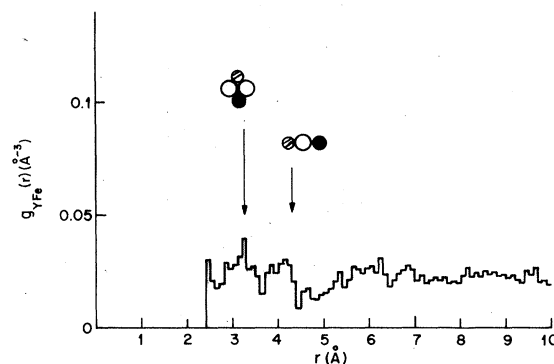


FIG. 5. Pair correlation function $g_{YFe}(r)$ which measures the density of Fe ions at a distance r from a Y ion in computer sample $C(d = 2.4 \text{ \AA})$. Shown in this and Figs. 6–10 are r values corresponding to simple planar geometric configurations as illustrated, where open circles represent oxygen ions, closed circles iron, and hatched circles yttrium.

β ions in the material. For continuum YIG we can use the fact that $\rho \approx (\frac{1}{12}) \text{ \AA}^{-3}$ and $c_Y = \frac{3}{20}$, $c_{Fe} = \frac{5}{20}$, and $c_O = \frac{12}{20}$ to obtain specific values. Since it is these values which we expect the correlation functions for the discrete model to approach at very large separations r we write them in the form

$$\begin{aligned} g_{\alpha Y}(r \rightarrow \infty) &\approx \frac{1}{80} = 0.0125, \quad \alpha = \text{Y, Fe, O} \quad , \\ g_{\alpha Fe}(r \rightarrow \infty) &\approx \frac{1}{48} \approx 0.021, \quad \alpha = \text{Y, Fe, O} \quad , \\ g_{\alpha O}(r \rightarrow \infty) &\approx \frac{1}{20} = 0.05, \quad \alpha = \text{Y, Fe, O} \quad . \end{aligned} \quad (6)$$

in units of Å^{-3}

Since quite generally $g_{\alpha\beta}(r)c_{\alpha} = g_{\beta\alpha}(r)c_{\beta}$ it is only necessary for YIG to calculate the six correlation functions $g_{YO}(r)$, $g_{FeO}(r)$, $g_{YFe}(r)$, $g_{YY}(r)$, $g_{FeFe}(r)$, and $g_{OO}(r)$ to obtain the complete pair-correlation information. In the actual computer summation we sample over spherical shells of radius r and thickness 0.1 \AA . However, since the cluster sample has a well-defined spherical boundary it is *not* necessary to re-

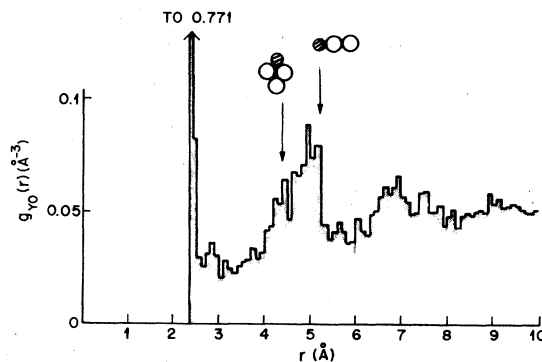


FIG. 6. Same as Fig. 5 but for correlations $g_{YO}(r)$ or oxygen density from an yttrium.

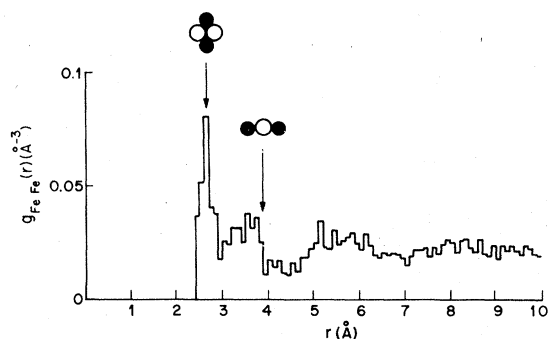


FIG. 7. Same as Fig. 5 but for correlations $g_{\text{FeFe}}(r)$ of iron-iron density.

strict our sums to A ions more than a distance r from the surface. It is easy to incorporate into the computer program the necessary geometrical correction to allow for the sampling of an incomplete r -radius shell near the surface and thereby to incorporate *all* α and β ions into the averaging process. This contrasts with the situation for the EFG computation in which only sites well inside the cluster could be sampled. Accordingly the resulting statistics are quite good particularly at larger r values; they are worst for $g_{\text{YY}}(r)$ because of the low relative concentration of Y in the material.

The results for $g_{\alpha\beta}(r)$ for r out to 10 Å are shown in Figs. 5–10. The correlation functions for the cluster models A and B differ significantly only in the case of iron-iron correlations with $r \leq 4$ Å. In Fig. 11 we show for comparison these near-neighbor iron-iron correlation results for the three clusters A , B , and C . The statistics are poor at very small radius ($r \leq 2$ Å) in Figs. 11(a) and 11(b) because the number of such pairs, being proportional to r^2 , is again quite small within the cluster sample.

Certain obvious planar geometrical configurations of the hard sphere components can be correlated with features in the correlation histograms. Perhaps the most impressive, in Figs. 7 and 11, is the markedly

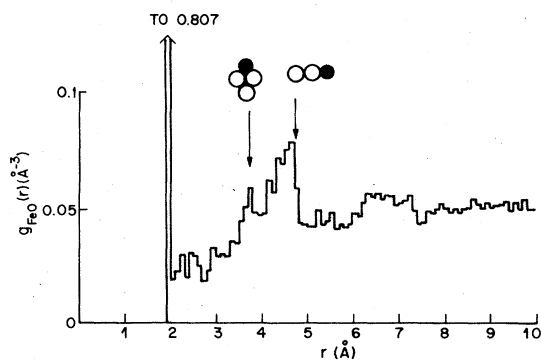


FIG. 8. Same as Fig. 5 but for correlations $g_{\text{FeO}}(r)$ of oxygen density from an iron.

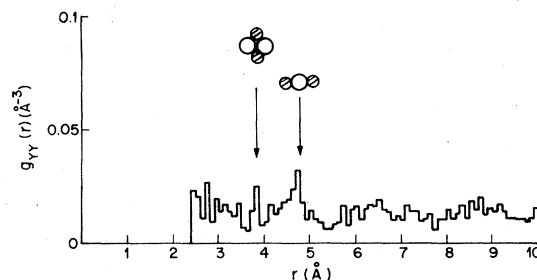


FIG. 9. Same as Fig. 5 but for correlations $g_{\text{YY}}(r)$ of yttrium-yttrium density.

enhanced occurrence in the cluster samples of iron-iron separations corresponding to the closest planar approach normal to the line of centers between two touching oxygen spheres. This coordination corresponds to an iron-oxygen-iron bond angle of approximately 90° and, in superexchange theory,¹³ gives rise to *ferromagnetic* interactions between the magnetic ions involved. On the other hand these ferromagnetic contributions are likely to be small in magnitude compared with the antiferromagnetic superexchange arising from bond angles closer to 180° .

VI. BOND ANGLES AND SUPEREXCHANGE

In crystalline YIG the overwhelmingly dominant exchange is antiferromagnetic and arises via superexchange through a single-anion bond (iron-oxygen-iron) with a bond angle of $7^\circ 126.6^\circ$. Each tetrahedral ferric ion has four such nearest-neighbor (nn) bonds, and each octahedrally coordinated iron has six. In the computer model C for amorphous YIG there exists a complete spectrum of iron-oxygen-iron bond angles θ for singly bonded ions ranging from $\theta = 76^\circ$ (corresponding to the minimum Fe-Fe separation of 2.4 Å) to 180° . Since we anticipate that only single-anion bonds will lead to significant magnetic exchange contributions, and since theoretically^{13,14} we

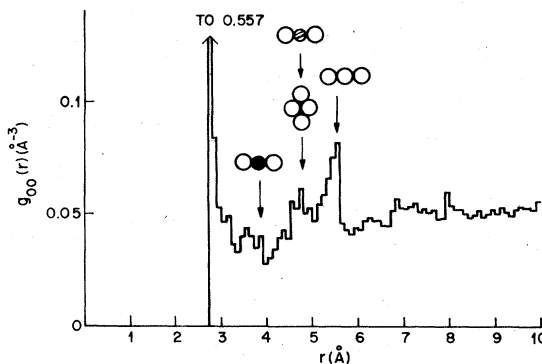


FIG. 10. Same as Fig. 5 but for correlations $g_{\text{OO}}(r)$ of oxygen-oxygen density.

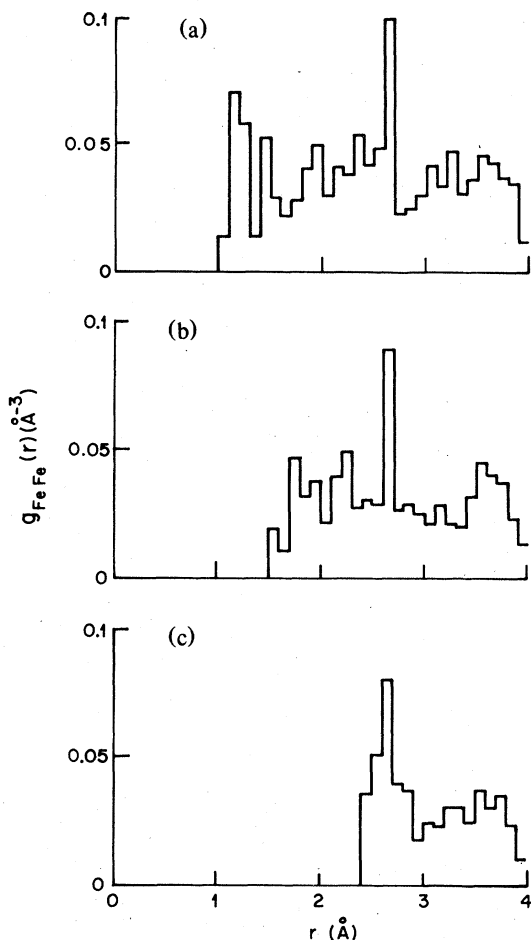


FIG. 11. Pair correlation function $g_{\text{FeFe}}(r)$ out to $r=4 \text{ \AA}$ for the three computer model samples *A*, *B*, and *C* defined in Table I [(a)-(c), respectively].

know the qualitative variation of superexchange with bond angle, a determination of the probability distribution $p(\theta)$ of these bond angles in the glass is important in building any serious model for the magnetic properties.

In order to sample the bond angle distribution $p(\theta)$ we examine the local environment about all Fe ions which are more than 4 \AA from the cluster surface (a 180° bond leads to an iron-iron separation of 3.9 \AA). A total of more than 200 bonds are involved and give the histogram for bond angle shown in Fig. 12. For those ferric ions involving bridging bonds with $\theta < 87.6^\circ$ some 40% (shown shaded in Fig. 12) are equally bridged by two oxygens, enhancing their superexchange contributions by a factor 2. The bond angle distribution is peaked fairly strongly in the $76 < \theta < 90^\circ$ region. In particular, the distribution of Fig. 12 is to be compared with the δ function at $\theta = 126.6^\circ$ expected in this context for crystalline YIG.

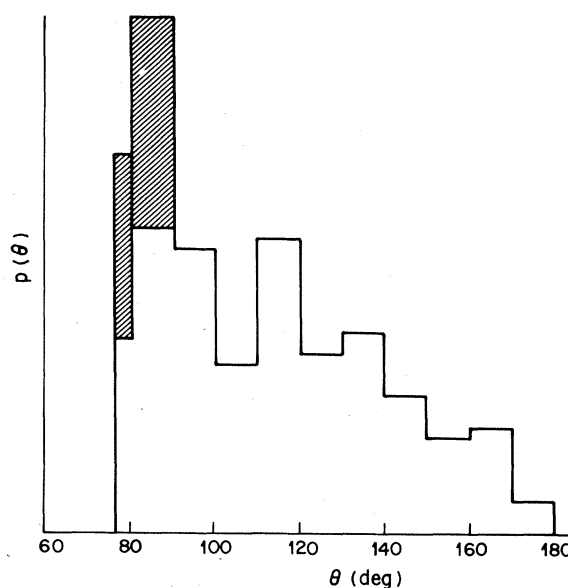


FIG. 12. Histogram for the probability distribution $p(\theta)$ of Fe-O-Fe bond angles θ in computer model *C*. For iron pairs with $\theta < 90^\circ$ a significant fraction (shaded in the histogram) have equal bridging paths via two oxygens, enhancing the exchange contribution for these by a factor of 2.

Since, for $\text{Fe}^{3+} (3d^5)$ we anticipate^{13,14} the presence of an antiferromagnetic direct contribution to exchange (via e orbitals) in addition to the ferromagnetic superexchange contribution at or near $\theta = 90^\circ$, it is not immediately obvious that the resultant total exchange parameter $J(\theta)$ becomes ferromagnetic at any angle. Materials with $\text{Fe}^{3+}\text{-O}^2\text{-Fe}^{3+}$ bonds near 90° have not been well studied. A few are known,¹⁵⁻¹⁸ such as $\alpha\text{-NaFeO}_2$ (with $\theta = 101^\circ$) and CuFeO_2 ($\theta = 96^\circ$), but no separate determination of the relevant exchange contributions seems to have been made in either case. Nevertheless, the fact that these materials are layer structures in which the in-plane exchange $J(\theta \sim 90)$ is expected to dominate, and that no long-range magnetic order exists in either above 14°K suggests that, regardless of its sign, $|J(\theta \sim 90)|$ is not larger than a few percent of that $[J(\theta = 126.6)]$ existing in crystalline YIG. The angle $\alpha = |\theta - 90|$ at which superexchange changes sign does vary a little with cation and anion type but is typically of order $10\text{--}20^\circ$. Assuming that the superexchange term dominates $J(\theta)$ in amorphous YIG we therefore expect an exchange distribution of the qualitative form shown in Fig. 13(a). Combining this with $p(\theta)$ from Fig. 12 now allows us to sketch the qualitative form expected for the probability distribution of exchange $p(J)$ in amorphous YIG. It is shown in Fig. 13(b).

Let us now examine the distribution of nearest-neighbor magnetic ions (defined as single-ion bridged magnetic neighbors) about the iron sites. From clus-

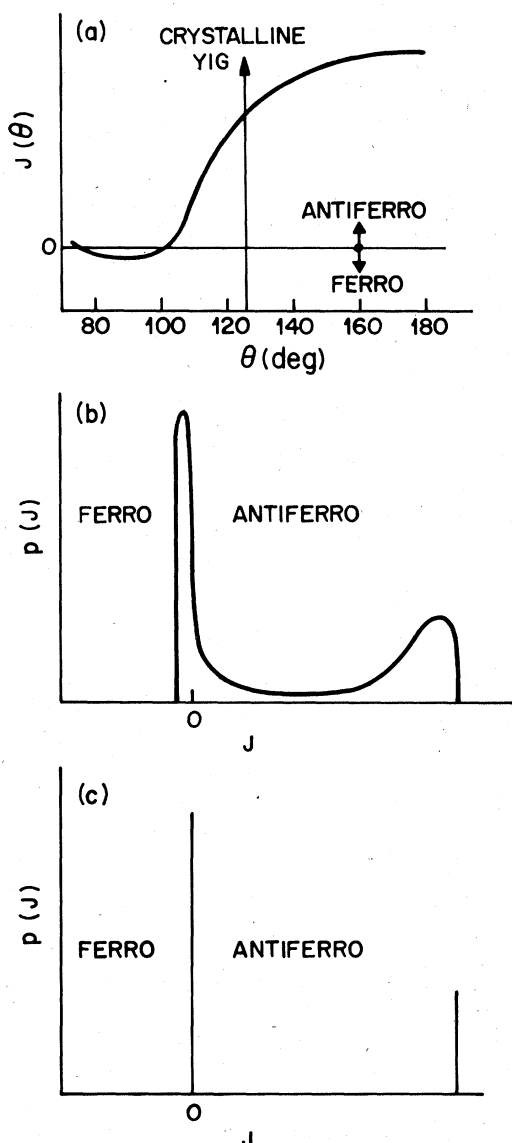


FIG. 13. (a) Qualitative form expected for Fe-O-Fe superexchange as a function of bond angle θ . (b) Qualitative form of the probability distribution $p(J)$ of exchange J in amorphous YIG. (c) Probability distribution of exchange in a translationally invariant lattice which is only partly filled with magnetic atoms, exchange $J \neq 0$, arising only from magnetic atoms on nearest-neighbor sites.

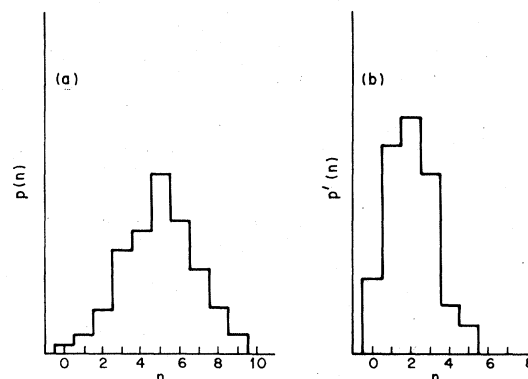


FIG. 14. (a) Probability $p(n)$ that a magnetic ion in amorphous YIG model C has n single-anion bonded magnetic nearest neighbors. (b) Probability $p'(n)$ that a magnetic ion in amorphous YIG model C has n "strongly magnetically interacting" nearest neighbors, defined as neighbors for which bond angle θ is greater than 115° .

ter model C we compute the probability $p(n)$ that a ferric ion has n magnetic nearest neighbors about it. This function is shown in Fig. 14(a). It peaks at $n=5$ but within our limited sample we do find one site with $n=0$ and, at the other extreme, two with $n=9$.

From the distribution $p(J)$ of Fig. 13(b) it is evident that, at least in lowest order, amorphous YIG behaves magnetically like a dilute antiferromagnet. If, for example, we take a lattice with translational invariance and randomly fill a fraction x of its sites with magnetic ions and the rest with nonmagnetic ions then, assuming only a nn antiferromagnetic exchange to be nonzero, the distribution function $p(J)$ takes the double δ function form of Fig. 13(c). The comparison with Fig. 13(b) is informative and we can take the analogy further.

If we consider all iron pairs with bond angle θ greater than say 115° to be "strongly" interacting [see Fig. 13(a)] and those with $\theta < 115^\circ$ to be weakly interacting, then we can compute the probability $p'(n)$ that a ferric ion has n "strongly interacting" nearest neighbors about it. This function is shown in Fig. 14(b) and, normalized to unity, is also given in Table II. It is peaked at $n=2$ and has no instances in our sample of coordinations greater than $n=5$. We now

TABLE II. Normalized probability distribution $p'(n)$ of "strongly antiferromagnetic" nearest neighbors; (A) in amorphous YIG and (B) in a 25%-filled body-centered cubic lattice.

Number of Neighbors	$n=0$	1	2	3	4	5	6	7	8
(A) $p'(n)$	0.10	0.27	0.30	0.23	0.06	0.04	0.00	0.00	0.00
(B) $p'(n)$	0.10	0.27	0.31	0.21	0.09	0.02	0.00	0.00	0.00

attempt to fit this distribution with a normalized binomial expansion of $[(1-x) + x]^m$, i.e., $p'(0) = (1-x)^m$, $p'(1) = mx(1-x)^{m-1}$, etc., which is appropriate for a lattice of coordination number m which is $100x\%$ filled with magnetic atoms. As shown in Table II the distribution $(0.75 + 0.25)^8$ provides an excellent representation of the computer distribution. It follows that the magnetic properties of amorphous YIG should, in some low order, be similar to that of a dilute (25% filled) body-centered cubic lattice of $S = \frac{5}{2}$ antiferromagnetically interacting spins.

The literature on dilute ferromagnets and antiferromagnets is already extensive but it is not the purpose of the present paper to pursue the above analogy in detail. Suffice it to say that, since the critical concentration (percolation limit) in a bcc lattice below which long-range order cannot exist even at absolute zero is about 22%,¹⁹ the situation for amorphous YIG

corresponds to a system close to critical concentration. This would account nicely for the very low transition temperature observed compared with that of crystalline YIG. Also, since the antiferromagnetic exchange interactions are so large compared with the ferromagnetic ones (which have been completely neglected in the dilute system analogy) any occurrence of spin-glass phenomena is unlikely. Frustration is at most very weak if only nearest-neighbor irons are magnetically important as assumed, and the ordered phase is therefore probably antiferromagnetic in the amorphous sense.²⁰

ACKNOWLEDGMENT

It is a pleasure to acknowledge many valuable discussions with M. Eibschutz throughout the course of this work, particularly with respect to an interpretation of the Mössbauer quadrupole data.

¹For a recent review see J. L. Finney, in *The Structure of Noncrystalline Materials*, edited by P. H. Gaskell (Taylor and Francis, London, 1977).

²A. M. Glass, M. E. Lines, K. Nassau, and J. W. Shiever, *Appl. Phys. Lett.* **31**, 249 (1977).

³A. M. Glass, K. Nassau, and J. W. Shiever, *J. Appl. Phys.* **48**, 5213 (1977).

⁴E. M. Gyorgy, K. Nassau, M. Eibschutz, J. V. Waszczak, C. A. Wang and J. C. Shelton, *J. Appl. Phys.* **50**, 2883 (1979).

⁵C. H. Bennett, *J. Appl. Phys.* **43**, 2727 (1972).

⁶See for example R. W. Cochrane, R. Harris, and M. Plischke, *J. Non-Cryst. Solids* **15**, 239 (1974).

⁷S. Geller and M. A. Gilleo, *J. Phys. Chem. Solids* **3**, 30 (1957).

⁸M. A. Gilleo and S. Geller, *Phys. Rev.* **110**, 73 (1958).

⁹G. S. Cargill, *Solid State Phys.* **30**, 227 (1975).

¹⁰T. C. Gibb, *Principles of Mössbauer Spectroscopy* (Chapman and Hall, London, 1975), p. 30.

¹¹S. N. Ray and T. P. Das, *Phys. Rev. B* **16**, 4794 (1977).

¹²S. N. Ray, T. Lee, T. P. Das, R. M. Sternheimer, R. P. Gupta, and S. K. Sen, *Phys. Rev. A* **11**, 1804 (1975).

¹³P. W. Anderson, in *Magnetism*, edited by G. T. Rado and H. Suhl (Academic, New York, 1963), Vol. 1, Chap. 2.

¹⁴See for example J. B. Goodenough, *Magnetism and the Chemical Bond* (Interscience, New York, 1963).

¹⁵T. Ichida, T. Shinjo, Y. Bando, and T. Takada, *J. Phys. Soc. Jpn.* **29**, 795 (1970).

¹⁶C. A. Taft, D. Raj, and J. Danon, *Phys. Status Solidi B* **64**, 111 (1974).

¹⁷A. H. Muir and H. Wiedersich, *J. Phys. Chem. Solids* **28**, 65 (1967).

¹⁸A. H. Muir, R. W. Grant, and H. Wiedersich, in *Proceedings of the Conference on Applied Mössbauer Effect, Tihany, 1969*, edited by I. J. Gruverman (Plenum, New York, 1971), p. 557.

¹⁹G. S. Rushbrooke and D. J. Morgan, *Mol. Phys.* **4**, 291 (1961).

²⁰J. M. Coey, *J. Appl. Phys.* **49**, 1646 (1978).